C.E. SACLAY
DSM

SERVICE DE PHYSIQUE NUCLEAIRE

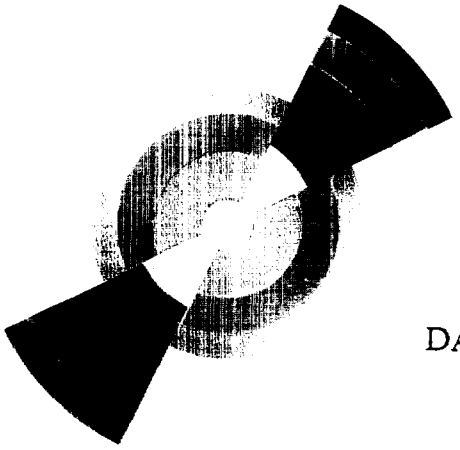

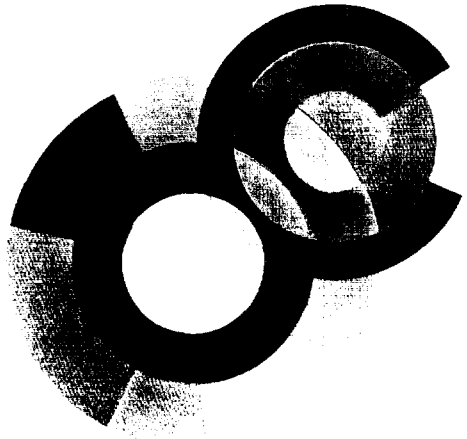

DAPNIA-SPhN-96-18

06/1996

Pseudoscalar meson photoproduction: from known to undiscovered resonances

B. Saghai and F. Tabakin

DAPNIA

Le DAPNIA (**D**épartement d'**A**strophysique, de physique des **P**articules, de physique **N**ucléaire et de l'**I**nstrumentation **A**ssociée) regroupe les activités du Service d'Astrophysique (SAp), du Département de Physique des Particules Elémentaires (DPhPE) et du Département de Physique Nucléaire (DPhN).

Adresse : DAPNIA, Bâtiment 141
CEA Saclay
F - 91191 Gif-sur-Yvette Cedex

Submitted to the Physical Review C

Pseudoscalar meson photoproduction: from known to undiscovered resonances

Bijan Saghai
Service de Physique Nucléaire, CEA/DSM/DAPNIA, Centre d'Etudes de Saclay, F-91191 Gif-sur-Yvette, France

Frank Tabakin*
Department of Physics & Astronomy, University of Pittsburgh, Pittsburgh, PA 15260
(June 27, 1996)

Abstract

The role of dynamics in spin observables for pseudoscalar meson photoproduction is investigated using a density matrix approach in a multipole truncated framework. Extraction of novel rules for $\gamma p \to \pi^+ n$, $K^+\Lambda$ and ηp reactions based on resonance dominance, and on other broad and reasonable dynamical assumptions, are discussed. Observables that are particularly sensitive to missing nucleonic resonances predicted by quark-based approaches, are singled out.

PACS: 25.20Lj, 14.40.Aq, 14.20.Gk, 24.70.+s

I. INTRODUCTION

Determination of the dynamics underlying pseudoscalar meson photoproduction has been a major challenge in hadronic physics for several decades. This challenge persists because: *i)* data remain scarce and of rather poor quality (except perhaps for the pion production case); and *ii)* the most advanced approaches, based on effective Lagrangian formalisms, embody entities not calculable *via* a fundamental theory, and hence require free parameters.

Intensive experimental effort at the Continuous Electron Beam Accelerator Facility (CEBAF), the Electron Stretcher Accelerator (ELSA), the European Synchrotron Radiation Facility (ESRF), the Laser Electron Gamma Source (LEGS) and at the Mainz Microtron (MAMI) are, or will soon be, providing copious and accurate data. One major anticipated advance is the measurement of single and double polarization observables. Simultaneously, phenomenological theories are becoming more sophisticated. Nevertheless, for kaons, and to a lesser extent for η and π photoproduction, a unique determination of the underlying dynamics is not anticipated because of possible contributions from a rather large number of resonances to the reaction mechanism.

The present work is motivated by an effort to ameliorate this awkward situation. We offer a potentially useful link between forthcoming polarization data and phenomenological analysis. In generating this link, we start from the model independent rules of Ref. [1]. In applying those rules to specific reactions, we invoke some broad and reasonable dynamical assumptions. These assumptions are: (1) the multipole amplitudes can be truncated, based on the centrifugal barrier; (2) multipole amplitudes are resonance dominated; and (3) the background and non-resonant contributions are small and structureless. Some of these are bold assumptions, but they do allow us to generate guidelines for resonance searching, prior to a full-fledged dynamical calculation. Thus, the purpose of this paper is to extend our earlier study [1] of *nodal structure* to isolate specific dynamical features.

Each pseudoscalar meson photoproduction case ($\gamma N \to \pi N$, KY, ηN), is known to have different characteristics. Pion photoproduction is the best understood channel. It has the advantage of being dominated by *only* one nucleonic resonance Δ_{33}. We show later that our analysis of spin observables agrees with the results of the best available phenomenological formalisms and sheds some light on further developments.

Among the three pseudoscalar meson production processes, the reaction mechanism for strangeness production is the most complicated and hence understood the least. This reaction has been discussed in detail in a previous paper [2]. For this reaction, we now provide more information by focusing on very recent polarization data and show how our nodal trajectory analysis deepens understanding of recent phenomenological models.

Finally, we study the η production case. Using recent experimental and theoretical results, we show here how the η production process might be used to search for missing, or undiscovered, resonances. [1] These resonances are predicted [3] by quark-based models [3–5]

---

[1]Missing, or undiscovered, resonances have been investigated by several authors. For illustration, we refer only to recent papers by Capstick and Roberts [3,4], which contains references to other relevant works.

to couple only weakly, if at all, to πN systems, but significantly to the ηN channel, which enhances interest in η production.

In Section II, the general structure of the cross section and all fifteen single and double polarization observables is presented. The notion of nodal trajectories is illustrated and applied to specific cases in Section III. Our conclusions are presented in Section IV.

II. SPIN OBSERVABLES IN A MULTIPOLE TRUNCATED BASIS AND DYNAMICAL RULES

The general rules for the sixteen observables, derived from a density matrix approach, are described in detail in Ref. [1] (FTS). From that work, we recall that the Legendre classes of the sixteen observables, which are labeled by $\mathcal{L}_0$, $\mathcal{L}_{1a}$, $\mathcal{L}_{1b}$, and $\mathcal{L}_2$, are:

$$\mathcal{L}_0(\mathcal{I}; E; C_{x'}; L_{x'}),\ \mathcal{L}_{1a}(P; H; C_{z'}; L_{z'}),\ \mathcal{L}_{1b}(T; F; O_{x'}; T_{x'}),\ \mathcal{L}_2(\Sigma; G; O_{z'}; T_{z'}).$$

In the above list, as explained in Table I, the first entry in each class is the cross-section or a single polarization observable ($\mathcal{I}, P, T, \Sigma$); the others are all double polarization observables, which appear ordered as Beam-Target (E, H, F, G), Beam-Recoil ($C_{x'}, C_{z'}, O_{z'}, O_{x'}$); with the last entry in each class being the Target-Recoil observables ($L_{x'}, L_{z'}, T_{x'}, T_{z'}$). The polarization asymmetries range from -1 to $+1$. The angular dependence of the above observables are determined by expressing the four helicity amplitudes $H_i(\theta)$ ($i = 1 \cdots 4$) in terms of Wigner rotation functions, with θ denoting the produced meson's center-of-mass angle. It is then simple to deduce that each $\mathcal{L}_M$ class observable can be expanded in a series of associated Legendre functions $P_{LM}(\cos\theta)$.

Rules concerning spin observables were discussed by FTS, based on the possible truncation of helicity or multipole amplitudes. The advantage of expanding the meson photoproduction amplitudes into multipoles $E_\ell^\pm, M_\ell^\pm$ is that the orbital angular moment, ℓ, of the final *meson-baryon* state can be used to reduce the number of amplitudes, based on the existence of a centrifugal barrier. Of course, this truncation does not include the possibility of dynamical effects, which could magnify selected orbital states. For example, a resonance could emphasize a particular partial wave or competing effects could attenuate selected waves. However, it is just the deviation from ordinary centrifugal-dominated behavior of spin observables and the dominant role of baryonic resonances that allow spin observables to serve as excellent indicators of special dynamical effects.

Spin observables organized by Legendre class and expressed as profile functions[2] are expanded in the following forms. For members of the Legendre class $\mathcal{L}_0$, the form is:

$$\mathcal{O} \equiv \sum_{L \geq 0} A_L P_L(\cos\theta) \equiv \sum_{m \geq 0}^{n} a_m \cos^m \theta.$$

---

[2]Profile functions [1] are the product of the spin observable times the cross-section function $\mathcal{I}$, with the cross-section given by $\sigma(\theta) = (q/p)\mathcal{I}$, where p and q denote the initial and final state c.m momenta. Profile functions are proportional to bilinear products of amplitudes.

For members of the Legendre class $\mathcal{L}_{1a}$ or $\mathcal{L}_{1b}$, the form is:

$$\mathcal{O} \equiv \sum_{L\geq 1} A'_L P_{L1}(\cos\theta) \equiv \sin\theta \sum_{m\geq 0}^{n} a'_m \cos^m\theta.$$

For members of the Legendre class $\mathcal{L}_2$ the form is:

$$\mathcal{O} \equiv \sum_{L\geq 2} A''_L P_{L2}(\cos\theta) \equiv \sin^2\theta \sum_{m\geq 0}^{n} a''_m \cos^m\theta.$$

The coefficients a_m, a'_m, a''_m can be expressed in terms of the basic multipole amplitudes. The manner in which a specific multipole contributes to these coefficients, and the possibility that the associated polynomial can have nodes, are the major features that we exploit in this paper to deduce definitive manifestations of underlying hadron dynamics. For example, *the condition for nodes, θ_0, in a spin observable, aside from endpoint (0° & 180°) zeroes, is* $\sum_{m\geq 0} a_m \cos^m\theta_0 = 0$.

For example, under the assumption that the $a_{m\geq 3}$ coefficients can be neglected, one needs to consider the quadratic equation $a_2x^2 + a_1x + a_0 = 0$ ($x = \cos\theta$), which has two solutions: $x_{1,2} = [-a_1 \pm (a_1^2 - 4a_0a_2)^{1/2}]/2a_2$. Nodes occur if a root is real and less than 1 in magnitude. To get real solutions, we need $a_1^2 \geq 4a_0a_2$. For $a_1^2 = 4a_0a_2$, we can get two equal solutions $x_1 = x_2 = -a_1/2a_2$; if these solutions are less than 1 in magnitude, then the observable has a non-sign-changing zero (NSC), not a sign-changing (SC) node. That locates the bifurcation point, which is the energy at which double nodes first set in. One can also generate conditions on the derivative of the profile function with respect to θ, which can be used to test if $m \geq 3$ coefficients can be neglected. Using such features, knowledge of nodes in a spin observable can provide definitive information about the $a_0, a_1, a_2 \cdots$ coefficients and thus about underlying multipole amplitudes and resonances. Of course, by fitting data directly over a range of energies, one can extract even more information from these coefficients.

To constrain dynamics and the basic multipole amplitudes, it is useful to express the coefficients a_m in terms of the electric and magnetic multipoles. The basic idea here is that for each photoproduced meson there is a family of dominant resonances. Those resonances feed into the multipole amplitudes of the same quantum numbers, which, in turn, determine the polynomial coefficients, a_m. Once these are known, the general energy and angular dependence of all spin observables, along with associated nodes, can be specified. Thus, each meson has spin observables characterized by its driving resonances.

To illustrate the angular dependence and the energy evolution of nodes, the spin observable E, a typical $\mathcal{L}_0$ Legendre class observable, is shown in Fig. 1. At the lowest incident energy, E takes only positive values; with increasing energy, it assumes a zero value at one angle (a non-sign changing zero, NSC). As the energy increases that single zero bifurcates into two nodes (sign changing nodes, SC). The projection of these nodes into the *node position-energy* plane constitutes the *nodal trajectory.*

With this 3D-plot in mind, we would like to stress two features used extensively in this paper. *The polynomial behavior of the angular distribution of the observable and/or its nodal structure depends on the incident photon energy. Moreover, such dependence may (and often does) vary from one observable to the other in a manner characterized by the underlying resonances.* This remark can be applied to every pseudoscalar meson photoproduction reaction.

III. NODAL TRAJECTORY ANALYSIS

Expressions relating the coefficients a_m, a'_m and a''_m to electric and magnetic multipole amplitudes (truncated at $\ell \leq 2$) were obtained [6] for all sixteen observables ($\mathcal{O}$) using Mathematica. These observables are organized as $\mathcal{O}_M = \sin^M\theta \sum_{m\geq 0}^{n} a_m x^m$, with $x \equiv \cos(\theta)$, where θ is the meson-baryon final-state angle in the c.m. system and the label $M = 0, 1$, or 2, for Legendre class 0, (1a, 1b), or 2, respectively. In Appendix A, a sample result is presented for the target polarization profile function. The relevant $a_0 \cdots a_5$ coefficients are given as imaginary parts of bilinear products of multipole amplitudes. By examining the structure of this particular result, we can understand the general form of all spin observables, as displayed in Table II.

To understand the notation used in Table II, consider the a_0 for the target polarization profile given in Appendix A. Its first term involves the S-wave multipole E^0_+, which has a total angular momentum of $J = 1/2$, and can be designated as an $S_{2I,1} \equiv S$ amplitude, using the usual convention $L_{2I,2J}$. For convenience, we present the case of general isospin I. The E_1^- and M_1^- multipoles are P-wave amplitudes with $J = 1 - 1/2 = 1/2$ and thus are designated as $P_{2I,1} \equiv P$ amplitudes. Similarly, E_1^+ and M_1^+ are P-wave amplitudes with $J = 1 + 1/2 = 3/2$ and thus are designated as $P_{2I,3} \equiv P'$ amplitudes. For D-waves, we have E_2^- and M_2^- amplitudes with $J = 2 - 1/2 = 3/2$, designated as $D_{2I,3} \equiv D$ and E_2^+ and M_2^+ amplitudes with $J = 2 + 1/2 = 5/2$, designated as $D_{2I,5} \equiv D'$ amplitudes.

The first term of a_0 in Appendix A involves interference between S- and P-waves of $J = 3/2$. To highlight that feature, we abbreviate that term as: "SP'," where the prime indicates again that the P-waves are of the $P_{2I,3}$ type. The remaining terms in a_0 for T involves P- and D- wave interference; they include $P_{2I,1}$ (M_1^-) interfering with $D_{2I,3}$ and $D_{2I,5}$ terms and also $P_{2I,3}$ (E_1^+ & M_1^+) interfering with $D_{2I,3}$ (E_2^- & M_2^-) and $D_{2I,5}$ (E_2^+ & M_2^+) terms. These terms are abbreviated as "$P_{2I,i}D_{2I,j}$" where i takes on the P-wave $2J$ values of 1 and 3, and j the D-wave $2J$ values of 3 and 5.

For the a_1 term of the target polarization, there are "$SD_j \equiv SD \oplus SD'$" terms, e.g. S & D interference involving $J = 3/2$ and $J = 5/2$ D-wave multipoles. In addition, interference between $J = 1/2(P)$ and $J = 3/2(P')$, is designated as a "PP'" contribution. Terms that involve $J = 3/2(E_2^-$ & $M_2^-)$ interference with $J = 5/2(E_2^+$ & $M_2^+)$ D-waves, are expressed in Table I as "DD'." Terms in a_2 involving P-waves of the same angular momentum, albeit of different electric or magnetic multipole character, such as $E_1^+ M_1^{+*}$, are denoted by a single letter "P'." For corresponding D-wave terms, $E_2^{\pm} M_2^{\pm *}$, for $J = 2 \pm 1/2$ cases, we enter a single letter: $D_{2I,3}$ & $D_{2I,5} \equiv D_{2I,j}$; where $j = 3, 5$ in Table II.

At this stage, we hope the compact notation used in Table II to describe the general structure of the coefficients a_m is clear, since it is essential for the rest of our paper. Note that there is an odd/even parity rule for the a_m terms in Table II. For example, the a_0 for the target polarization entry involves $\ell = 0$ & 1 plus $\ell = 1$ & 2 interference–which are odd terms. The next term, a_2, is an even term which involves $(\ell = 1) \times (\ell = 1)(P')$ and $(\ell = 2) \times (\ell = 2)(D_{2I,j})$ terms, plus three other manifestly even interference terms. That pattern, which appears throughout the table, is clearly a reflection of the underlying tensorial and parity character of each spin observable. Another important feature is the location of the E_0^+ multipole amplitude, which is indicated by the boxed terms in Table II: interference and also magnitude, "S", type terms appear in these boxes. As we will see in Sec. III.A.3,

this S-wave amplitude if quite large, will make the a_m in which it appears dominant. Terms that involve interference between this sizable, S-wave amplitude and particular P- and D-waves, have amplified values of the a_m in which that S-wave occurs. If the S-wave interferes with a resonant P- or D-wave amplitude, then great magnification of that term can occur; which can cause dramatic changes in nodal and polynomial structure. It is such a mechanism that we seek to isolate and use to magnify the role of as yet unseen resonances!

By identifying different resonances, according to their angular momentum and spin, with the relevant multipoles, the expressions for the observables summarized in Table II can be used to anticipate the role of resonances on spin observables. There are basically two types of terms in Table II (see Appendix A): those coming from a single resonance ($\propto |E_\ell^\pm|^2$, $|M_\ell^\pm|^2$, $E_\ell^\pm \cdot M_\ell^\pm$) and those arising from interference terms between two resonances. Here we begin to identify amplitudes with resonances; indeed, our key point is that by *assuming that amplitudes are dominated by resonances*, we can anticipate the angle and energy dependence of spin observables and their sensitivity to particular resonances.

One needs to be careful about treating the isospin. Although Table II refers only to a fixed isospin I, the Table generalizes to the $I = 1/2$ & $3/2$ case, as occurs for pions. The interpretation of the P- and D-wave interference term "PD," maps to sums over isospin: namely,

$$PD \to \sum_{I,I'} P(I) \cdot D(I');$$

whereas, the diagonal-type term "D" becomes [3]

$$|D|^2 \to \sum_{I,I'} |D(I) + D(I')|^2.$$

We can now apply the general rules for the structure of the spin observables to different pseudoscalar mesons.

A. Dynamical Rules

In this Section, we give examples of the angular distribution of the polarization observables in $\gamma p \to \pi^+ n, \eta p$, and $K^+\Lambda$ processes, in order to gain insight into how the above general rules help to reveal the basic dynamics.

1. Pion

Pion photoproduction is by far the most investigated [7] of these reactions. Despite this attention, complete angular distribution data for polarization observables remain scarce. Experiments recently completed at Bonn [8,9] and Brookhaven [10] will soon greatly enlarge the data base. Here, we investigate the preliminary results from the PHOENICS Collaboration [8].

---

[3]Isospin factors and relevant phases have been incorporated into the amplitudes.

The target polarization asymmetry, T, at $E_\gamma^{lab} = 220$ MeV and 650 MeV for the reaction $\gamma\vec{p} \to \pi^+ n$ are shown in Fig. 2. The profile function for this $\mathcal{L}_{1b}$ Legendre class single spin observable can be expressed in the form $\sin\theta \times (a_0 + a_1 x + a_2 x^2 + \cdots)$. The polynomial coefficients a_m were adjusted to fit these data. The data at both energies, Fig. 2, are quite well reproduced by a second order polynomial, for the higher energy results the need for a third order polynomial is unclear. What can we learn from the fact that the data require a second order polynomial?

We now use Table II for the spin observable T. Based on the most recent phenomenological calculations, we assume zero $D' \equiv D_{1S}$ contribution. In that case, the entry for T in Table II shows the following coefficient structure:

$$\begin{aligned} a_0 &= SP' \oplus PD \oplus P'D, \\ a_1 &= P' \oplus D \oplus SD \oplus PP', \\ a_2 &= P'D, \\ a_3 &= 0. \end{aligned} \tag{3.1}$$

From the above, one sees that neglecting D' resonances leads to a second order polynomial. Moreover, to generate a nonzero a_2 the pion-nucleon system must have significant, and we assume resonant, $P'D$ contributions. Note the dominant Δ_{33} isobar is a $I = 3/2$, P' state. The presence of the Δ_{33} *and* spin-3/2 ($l = 2$) resonances (P' and D, respectively) are necessary to get $a_2 \neq 0$. Thus, evidence for an a_2 polynomial, under the assumption of zero D' terms, can shed light on the role of a D contribution.

Fitting the lower energy 220 MeV data with a second order polynomial, we find that $a_2 \simeq 2 \cdot a_1$; with $|a_2|$ slightly larger than $|a_0|$. Given that a_1 is the only coefficient containing a pure contribution from the dominant Δ_{33} resonance (the single P' term), the smallness of this coefficient implies that the other terms in a_1 interfere destructively with the P' term. Also the extra terms in a_0 compared to a_2, $SP' \oplus PD$, are slightly destructive, since we find that $|a_2|$ is slightly larger than $|a_0|$. Recall that to get a real node in a second order polynomial, we need $a_1^2 \geq 4a_0a_2$, which is not satisfied here; hence, this observable has its nodeless behavior despite the Δ_{33} resonance.

This absence of nodes at 220 MeV also implies that resonances other than the Δ_{33} are required by the data, as is already known from existing models (see, for example Ref. [11]). In particular, the 220 MeV data yield values of the polynomial coefficients which, from the above structure, require contributions from spin 1/2 (S and P) and spin 3/2 (P' and D) nucleonic resonances. Again, we assume that the multipole amplitudes are resonance dominated, although it is possible that a background can play a significant role and should be included in a fully dynamical analysis.

At the higher energy 650 MeV, the absolute values of the coefficient a_0 for both the $n = 2$ and $n = 3$ polynomial fits are small. Without an a_0 term, the observable T has a $\sin\theta \times \cos\theta$ structure; hence, a node appears in T near $\approx 90°$ for small a_0. To obtain that small value of a_0 and the $\approx 90°$ node, the terms in the expression given above must interfere destructively, e.g. $SP' \oplus PD \oplus P'D \approx 0$.

Note that using Table II, if the data requires $n = 3$ terms, then besides the spin 1/2 and spin 3/2 resonances, the reaction mechanism would acquire contributions from a spin-5/2 resonance (D'). Such a resonance, at higher energies ($\geq$ 800 MeV), has been suggested

by Garcilazo and Moya de Guerra [11] in their extensive study of pion photoproduction using an effective-Lagrangian-based model which includes s-channel, spin-1/2 and spin-3/2 resonances (S, P, P', & D).

Although, we can learn from the above how to analyze the general structure of T for its resonance dependence, we also see from Table II that the target asymmetry T is not the best observable for investigating the role of spin-5/2 resonances (D'). From Table II, the Beam-Recoil ($C_{x'}, C_{z'}, O_{x'}, O_{z'}$); and Target-Recoil ($L_{x'}, L_{z'}, T_{x'}, T_{z'}$) double polarization observables offer much cleaner cases for that purpose. These observables can be classified in three groups according where a pure magnitude D' term occurs. For $C_{x'}\&L_{z'}$, "D" occurs in the $n = 5$ term; for $C_{z'}, L_{x'}, O_{x'}, \&T_{z'}$, "$D$" occurs in the $n = 4$ term; while $O_{z'}\&T_{x'}$ have the lowest occurrence of a "D"-in their $n = 3$ terms. The common feature to all of these double spin observables is not only that the highest power coefficient ($a_{n_{max}}$) is a *pure* D' state, but also that the $a_{n_{max}-1}$ coefficient depends *only* on the $P'D'$ interference terms. Given the dominant role played by the Δ_{33}-resonance (P'), the effect of the D' resonance is hence magnified in all of these observables, with evidence for a_2, a_3 terms in $O_{z'}\&T_{x'}$ offering the best choice among these double spin observables.

However, the most promising observables in looking for the effects of spin-5/2 resonances are, according to Table II, reached using a linearly polarized beam, e.g. the single polarization Σ and double beam-target G asymmetry. That conclusion is based on the fact that D' enters into the lowest order polynomial terms for these observables.

Having shown how Table II, provides a guide for resonance searching in pion photoproduction, we now turn to another example.

2. *Kaon*

Due to a large number of resonances and t-channel exchanges, the reaction mechanism for associated strangeness photoproduction is much more complicated [12–15] than for π and η photoproduction. However, in $K^+\Lambda$ (and η) channels only isospin $I = 1/2$ resonances can intervene, which is at least one simplification compared to the pion case.

The only published angular distribution data for polarization observables are the hyperon-recoil (P) asymmetry recently measured at ELSA [16]. In Figure 3 their results for the $\gamma p \to K^+\vec{\Lambda}$ channel at 1.2 GeV are shown. In Fig. 3(a), the results of our polynomial fit using the form: $P = \sin\theta \sum_{m=0}^{n} a_m x^m$, with $x \equiv \cos(\theta^K_{cm})$ are depicted for four polynomial orders ($n = 1, 2, 3$, and 4). The end points are required to be zero, by virtue of the helicity amplitude structure of this observable [1]. From Fig. 3(a), we infer that although an $n = 2$ polynomial gives an acceptable description of the data, the use of an $n = 3$ polynomial decreases the χ^2 by roughly a factor of 4, while there is no significant need for $n = 4$ terms. The structure of the P-asymmetry (see Table II), shows that evidence for an $n = 3$ polynomial implies the presence of spin-5/2 nucleonic resonance(s) (D') in the underlying dynamics.

To confront this finding with our present knowledge of the relevant reaction mechanism, we show in Fig. 3(b) the *predictions* of three recent phenomenological approaches [12–14] based on isobaric formalisms. These effective-Lagrangian-based models contain s-, u-, and t-channel exchanges. In a previous paper [2], we investigated the implications of these exchange channels on our nodal trajectory analysis. Here, we will concentrate on the s-channel nucleonic resonances. The s-channel content of the three models discussed here, can

be summarized as follows. The two first models by Adelseck-Saghai (AS) [12], and Williams, Ji, Cotanch (WJC) [13], include only spin-1/2 resonances. Namely, AS : $[P_{11}(1440)] \subset [P]$; WJC: $[S_{11}(1650),\ P_{11}(1710)] \subset [SP]$. While the most recent model from the Saclay-Lyon Group (SL), by David *et al.* [14], contains spin-1/2, spin-3/2 and spin-5/2 resonances: $[P_{11}(1440),\ P_{13}(1720),\ D_{15}(1680)] \subset [PP'D']$. From Fig. 3(b), and the χ^2 per point values (AS : 2.5, WJC : 1.9, SL : 1.5), we conclude that the *genuine* spin-5/2 resonance in the SL model is producing the anticipated a_3 effect discussed in the previous paragraph.

Note that the AS and WJC models reproduced the data with reasonable accuracy. The AS model *predicted* the existing (old) P-asymmetry data especially well, and the WJC model reproduces correctly all data included in their fitted data base. As discussed in a previous paper [2], the higher spin resonances missing in the AS and WJC models are mimicked by the $t-$channel exchanges, in line with the duality hypothesis. Nevertheless, as we anticipated [2], the P-asymmetry is basically a resonance driven entity. This resonance dominance is confirmed by the results shown in Fig. 3.

For further *illustration* of the role of the polynomial coefficients, we mention that the numerical values of the coefficients for the $n = 3$ polynomial fit to the Λ-polarization asymmetry in Fig. 3(a) satisfy the following relations, at the level of a few percent: $|a_0| \simeq |a_2|$ and $|a_1| \simeq |a_3|$. From Table II, we see that:

$$\delta_{02} \equiv |a_0| - |a_2| \propto SP_{1i} \oplus PD \equiv SP \oplus SP' \oplus PD,$$

and

$$\delta_{13} \equiv |a_1| - |a_3| \propto SD_{1j} \oplus PP' \equiv SD \ominus SD' \ominus PP'.$$

Let us now examine how our fit using the above $n = 3$ polynomial structure, which implies $\delta_{02} \simeq 0$ *and* $\delta_{13} \simeq 0$, can arise.

In a rather *complicated* reaction mechanism which includes S_{11}, P_{11}, P_{13}, D_{13}, and D_{15} nucleonic resonances, the above relations ($\delta_{02} \simeq \delta_{13} \simeq 0$) can be satisfied in one of the two following ways:

i) Strong interference effects : highly destructive interference occurs among the SP, SP', and PD terms, *and* also among SD, SD', and PP' terms.

ii) Weaker interference effects: if the contributions from P_{11} resonance(s) are negligible, then $\delta_{02} \propto SP'$ *and* $\delta_{13} \propto SD_{1j}$. In this case, $\delta_{02} \simeq 0$ is satisfied if contributions from $S-$ or $D-$ waves are negligeable. Moreover, either small SD *and* SD' or destructive interference between these two terms will ensure $\delta_{13} \simeq 0$.

Actually, the SL model (obtained within the most comprehensive phenomenological approach), is very close to the second of the above options and provides (almost) vanishing values for both δ_{02} *and* δ_{13} through simple and hence appealing mechanisms. Namely, in the SL model there are no S - and D -wave resonances, hence $\delta_{02} = 0$ and $\delta_{13} \propto PP'$. Moreover, in the SL model the relation $\delta_{13} \simeq 0$ is verified because the only P_{11} resonance (Roper resonance) has a very tiny overall coupling in the process $\gamma p \to P_{11} \to K^+\Lambda$; namely, the product of the initial state (electromagnetic production vertex) and the final state (strong decay vertex) coupling constants $G_{N^*} \equiv g_{\gamma pN^*} \cdot g_{K\Lambda N^*}$, ($N^* \equiv P_{11}$), comes out to be very small (see Ref. [14] Tables IX), as determined by fitting the relevant data (differential and total cross sections, the Λ-polarization asymmetry and the radiative capture branching ratio).

Our analysis hence explains the negligible role (see Ref. [14] Tables XII) played by the Roper resonance in the strangeness electromagnetic production reaction.

The above discussion provides a clear example of the significant role that our nodal approach can play in establishing links between data and dynamical models. More precisely, if the forthcoming polarization data, expected to be more accurate and contain more complete angular distributions, confirm the above analysis of the $n = 3$ polynomial coefficients, then future models could exclude the nucleonic S_{11} and P_{11} resonances from consideration, thereby decreasing considerably the number of candidate resonances, *and consequently*, the number of resonance sets to be investigated.

We now turn to the third case of pseudoscalar photoproduction and introduce its resonance structure.

3. Eta

New experimental facilities are or will soon be used to study η-photoproduction extensively. Recent low energy cross section measurements [17,18] have already provided insights into the dynamics of this process. At the present time, it seems to be established [19], *via* an effective Lagrangian approach including s-channel spin 1/2 & 3/2 nucleonic resonances and t-channel vector meson exchange processes, that the reaction mechanism, at least for $E_\gamma^{lab} \leq 800$, is dominated by two resonances: $S_{11}(1535)$ and $D_{13}(1520)$. These data, as well as more extensive preliminary data from ELSA [20,21] between threshold and 1150 MeV, have also been investigated [22] within a formalism based on an isobar model [22,23]. In this approach electric and magnetic multipole amplitudes are expressed in terms of various isospin-1/2 nucleonic resonances described by "relativized" energy-dependent Breit-Wigner forms, plus a smooth background including S- and P- waves. The role of the following resonances has been investigated: $S11(1535)$, $S11(1650)$, $P11(1440)$, $P11(1710)$, $P13(1720)$, $D15(1675)$, $D13(1520)$, $D13(1700)$, $F15(1680)$, $G17(2190)$. This isobaric approach of Ref. [22], which is less fundamental than the effective Lagrangian formalisms, has the advantage of allowing one to rather easily include higher spin resonances in the reaction mechanism. The results of this isobar model work [22] confirm the major role played by the $S11(1535)$ and $D13(1520)$ resonance. More reliable conclusions about the reaction mechanism up to 1.2 GeV await the release of final data.

Nevertheless, two main questions are worth investigating: *i)* Can the sub-threshold, but wide, Roper resonance play a significant role in the reaction mechanism, especially with respect to the forthcoming higher energy data [21] from Bonn? *ii)* Could this process be used to search for undiscovered and/or missing resonances[4] as predicted [3] by recent relativized pair-creation quark models?

To address these questions, we single out the most relevant dynamical sets of resonances. In Table III, we list all observables and, using Table II as input, we indicate the resonance dependence of the polynomial expansion coefficients for various sets of assumed resonance

---

[4]In this paper, we focus on the following resonances predicted by Capstick and Roberts [3]: P_{11}, P_{13}, and D_{15} with masses around 2 GeV, and non-vanishing decay amplitudes to the ηN channels.

amplitude scenarios. Since the η photoproduction is dominated by $S_{11}(1535)$ and $D_{13}(1520)$, we start from the SD resonant set, then we sequentially add in contributions from $P_{11} \equiv P$, $P_{13} \equiv P'$ and $D_{15} \equiv D'$. Thus, we consider the resonance scenarios of: only SD, resonances, then add in P to get SPD or P' to get $SP'D$, add in both spin 1/2 and 3/2 P-waves ($SPP'D$). Finally, with P, P', & D' all on, the resonance set is: $SPP'DD'$. This sequence of resonances has been generated by the following considerations: *i)* the main reasons for considering P_{11} are that, first it is desirable to identify observables which could reveal the role, if any, played by the Roper resonance $P_{11}(1440)$ in this reaction, and secondly to look for two of the missing P resonances with masses around 1.9 GeV; *ii)* for the P_{13} sector, it is desirable to find out which observables, if any, are suitable in searching for undiscovered resonances; *iii)* then a combination of these four family of resonances (*i.e.* $SPP'D$), and an additional contribution from a spin 5/2 resonance (D') is investigated. The need for such a spin-5/2 resonance (D') has already been anticipated in the case of pions [11], and shown in the case of kaons [14]. So, either a known or a missing D' high spin resonance might also appear in the η case in the comparable energy region. If so, the resonance set ($SPP'DD'$) in Table III should be considered in determining the best observable for seeing the D' effect in η photoproduction.

For each of the above η−nucleon resonance scenarios, we use Table II to restrict the relative magnitudes of the a_m coefficients for η photoproduction. In Table III, we summarize these η photoproduction results. [5] The relations in Table III are generated from Table II in the following manner: recall that S is the dominant resonance (85 to 90% of the η photoproduction cross-section) and then add in the other significant resonance D13. With just these two dominant resonances, we obtain vanishing values for some coefficients. We also obtain the order of the polynomial that can be generated by just these two resonances–the SD resonance set. Next, additional resonance scenarios are considered in the order SPD, $SP'D$, $SPP'D$, and finally $SPP'DD'$. At each step we obtain the possible order of the polynomial, along with some rules on the polynomial coefficients a_m. Most of the rules are based on the dominance of S and D amplitudes, followed by the secondary P and D-resonances. In addition, there is an additional arbitrary assumption made at times that interference terms are all constructive. This assumption is of course not always true; indeed, we saw some examples of destructive interference occur in the pion and kaon reactions. For those special times, the (unequality) relations between polynomial coefficients in Table III, provide only "upper" or "lower" limits on the coefficients, assuming constructive (or slight destructive) interferences. However, even in the case of highly destructive interferences, as discussed in pion and kaon Sections, our approach allows extracting significant informations on the dynamics of the investigated processes.

As an example of how to obtain Table III from Table II, consider the T term in Table II. The coefficients for T extracted from Table II, under the assumption of zero D', were presented earlier in Eq. 3.1. For the η case with just the SD dominant resonances, we see from Eq. 3.1, that $a_0 \equiv 0$, and that only a_1 is on, e.g. a polynomial of $n = 1$ order is obtained. These facts are entered in Table III in the T row and the $n = 1$ polynomial column. Footnote *d* presents the additional information that $a_0 = 0$ for this resonance scenario. In this way,

---

[5] Similar specializations of Table II could be generated for the π and K^+ cases.

all of Table III is generated.

Information stored in Table III for η photoproduction relates not only to the angular structure of observables, but also, since higher $n's$ enter with increasing energy, to their energy evolution. We now wish to address the question 'Can a previously undetected resonance drive one of these polynomial coefficients and dramatically alter the angular and energy dependence of specific spin observables?'

Let us begin by examining the cross-section part of Table III. From their cross-section data, Krusche *et al.* [18] concluded that only $S_{11}(1535)$ and $D_{13}(1520)$ resonances are required, which is also a feature of recent models [19,22]. The absence of P-waves, especially due to the Roper resonance, has been deduced by Krusche *et al.* [18] from their finding that a polynomial of the second order, with $a_1 \approx 0$, (within the experimental uncertainties), suffices to fit their cross-section data. Both SD and SPD resonance scenarios lead to such a second order polynomial form for the cross-section[6], however, for the case of just the SD resonance set one finds that $a_1 = 0$ from Table III. In contrast, a SPD set of resonances yields $a_0 > a_2 > a_1$, which suggests that in a reaction mechanism *dominated* by the SD set. introduction of an additional secondary P_{11} resonance (e.g., the SPD set) should yield a *small* a_1 coefficient, compared to a_0 and a_2. Finding clean evidence for a P_{11} resonance effect from cross-section data, in a situation where S and D resonances dominate, thus requires one to extract an a_1 coefficient from the data with a *significant* non-vanishing value (*within the associated experimental errors*). That is a quite difficult experimental task and hence suggests that we go beyond the cross-section in searching for P_{11} resonance effects.

There are observables that are more sensitive to P_{11} resonance(s) effects than the cross section. For example, consider the single target (T) or recoil (P) polarization asymmetries, as well as the double polarization beam-target observables H and F (with linearly or circularly polarized beams, respectively). All of these four spin observables share the property that both SD and SPD sets lead to first order polynomials, $\sin^M\theta(a_0 + a_1\cos\theta$, see Table III. In the case of the pure SD resonance set, we find that $a_0 = 0$; hence, a node at 90° is anticipated for all four of these observables. With the SPD resonance set, both coefficients of the first order polynomial are finite for all four of these observables, with $a_1 > a_0$, which means that these observables have one node at $\theta_0 \neq 90°$. The deviation of the node position from 90° depends on the ratio a_0/a_1 and therefore are sensitive measures of the importance of the P_{11} amplitude.

From among the four observables discussed above, the P and H asymmetries have a potentially useful property that all of the polynomial coefficients for P and H arise *exclusively* from interference terms, see Table II. Thus, the a_0 coefficients for P and H observables are particularly excellent ways to amplify P-wave (both P_{11} and P_{13}) effects, since they appear interfering with the two dominant S and D resonances in a_0.

For the four observables *T, P, H and F*, investigation of the $SP'D$ set is also very informative. Here, we are dealing with a second order polynomials with $a_1 >> a_0 > a_2$. Hence, besides the special sensitivity of a_0 to P-waves, this polynomial gets two roots and possibly two nodes. Thus, observation of double nodes in these observables, especially if they evolve

---

[6]The cross-section σ, is a $\mathcal{L}_0$ class observables: its profile function is $\mathcal{I}$ which, as indicated earlier, is defined by $\sigma \equiv (q/p)\mathcal{I}$.

rapidly with energy, would be strong indication of a P' resonance.

In summary, for the observables P, H, T, and F, the resonance sets SD, SPD, $SP'D$ lead to one node at 90°, and one node at $\theta \neq 90°$, and possibly two nodes, respectively. Direct experimental evidence of such nodes could be a way to reveal associated P and/or P' resonance dynamics.

For the $SPP'D$ case, we see from Table III, that two nodes are possible for the observables P, H, T, and F. In these cases, however, $a_2 \neq 0$ by itself (see Table II) implies contributions from P_{13} resonance(s), whether or not P_{11} resonances contribute.

The single photon polarization asymmetry, Σ, and the double polarization beam-target observable, $G, (\mathcal{P}_{lx}^{00})$ with linearly polarized beam, show no sensitivity to additional P_{11} resonances, since both SD and SPD sets generate first order polynomials for these observables, with $a_1 = 0$. Hence for both SD and SPD resonance sets, Σ, and G are nodeless. Adding a P_{13} to any of these sets ($SP'D$ and $SP'PD$) leads to $a_0 > a_1 \neq 0$, in which case Σ and G remain nodeless. Hence, Σ and G are particularly insensitive, especially in their nodal structure, to P' resonances. They are, however, quite sensitive to the addition of a D' resonance, since it opens the possibility of two nodes. A bifurcated nodal trajectory in either Σ or G , which involves going from zero to two nodes, especially if it occurs rapidly, could be striking evidence of a D' effect.

The beam-recoil asymmetries $O_{x'}(\mathcal{P}_{l0}^{0x'})$ (with linearly polarized beam) and the target-recoil $T_{x'}(\mathcal{P}_{0x}^{0x'})$ produce a first order polynomial for all resonance scenarios, except for the full case of $SPP'DD'$, wherein, the D' resonance enters. For these observables a node at 90 degrees occurs (since $a_0 \equiv 0$) assuming just the pure SD set. The SPD, $SP'D$, and $SPP'D$, scenarios all generate a one non-90 degree node situation. The full scenario set $SPP'DD'$, brings in a cubic polynomial, which suggests that these observables could have bifurcating nodal trajectories, for which the change from one to three node is driven by a D' resonance.

For the beam-recoil $C_{x'}(\mathcal{P}_{c0}^{0x'})$ (with a circularly polarized beam) and target-recoil $L_{x'}(\mathcal{P}_{0z}^{0x'})$ observables, we see from Table III that a polynomial of third order with $a_0 = a_2 = 0$ is obtained in the case of a pure SD resonance set. Thus $C_{x'}$ and $L_{x'}$ have 90 degree nodes in that limit.[7] Since $a_1 > a_3$ is also indicated for the pure SD case, a second node is unlikely. However, with the addition of P and P' resonances, these observables could acquire up to three nodes for all non-D' cases. Once a D' resonance enters, the polynomial jumps to fifth order, with five nodes possible.

Now consider the most complicated reaction mechanism presented in Table III; namely, the case of the full resonance scenario $SPP'DD'$. As can seen in Table II, the highest order coefficient for all observables is either a pure D' state ($C_{x'}$ $(\mathcal{P}_{c0}^{0x'})$, $L_{x'}$ $(\mathcal{P}_{0z}^{0x'})$, $C_{x'}$ $(\mathcal{P}_{c0}^{0x'})$, $L_{x'}$ $(\mathcal{P}_{0z}^{0x'})$, $O_{x'}$ $(\mathcal{P}_{l0}^{0x'})$, $T_{x'}$ $(\mathcal{P}_{0x}^{0x'})$, $O_{x'}$ $(\mathcal{P}_{l0}^{0x'})$, $T_{x'}$ $(\mathcal{P}_{0x}^{0x'})$), or a combination of pure D' state plus an amplification of it by the D resonance ($D' \oplus DD'$) ($d\sigma$, E $(\mathcal{P}_{cx}^{00})$, T $(\mathcal{P}_{0y}^{00})$, F $(\mathcal{P}_{cx}^{00})$, Σ $(\mathcal{P}_{l0}^{00})$, G $(\mathcal{P}_{lx}^{00})$). or just a DD' interference term–which is the case for P $(\mathcal{P}_{00}^{0y'})$, H $(\mathcal{P}_{lx}^{00})$. These last eight observables, by virtue of their DD' terms, allow the dominant D to overlap and hence magnify the role of a possible D' resonance. Thus they offer particularly suitable

---

[7]Both $C_{x'}$ and $L_{x'}$ must have an odd number of nodes according to the general helicity rules of Ref. [1].

observables for investigating the contributions of any known or missing $D' \equiv D_{15}$ resonances.

Finally, we emphasize that, since the relations among the polynomial coefficients displayed in Table III, often give clear information about the anticipated nodal and polynomial structures of the relevant observables, there is hope that the character of angular distributions and associated nodal structure might yield definitive evidence for specific resonances.

IV. SUMMARY AND CONCLUSIONS

Our analysis of the angular distribution of forthcoming polarization observable data and their special nodal trajectory and polynomial characteristics, within a multipole truncated basis, offers a potentially powerful means for investigating the underlying dynamics of pseudoscalar meson (π, K, η) photoproduction. This method provides a helpful guide for phenomenological dynamical approaches by singling out the appropriate families of nucleonic resonances required by existing data. Also, confronting this polynomial expansion analysis with existing phenomenological approaches, allows one to emphasize both the strong and weak points of such models and put forward suggestions for improvements. Moreover, this method promises to be a helpful guide in planning experiments to search for missing and/or yet undiscovered resonances, which constitutes a crucial test of quark-based descriptions [3–5] of baryon spectra.

While waiting for a new generation of precision data, we confronted our approach with both extant, but scarce, polarization data, and with the predictions obtained using recent phenomenological models. In the process, we learn some things. For example, for pion photoproduction, we focused on the polarized target asymmetry T data [8], and showed that our approach incorporates some of the established facts; namely, that the reaction is dominated by the Δ_{33} resonance with non-negligible contributions from other spin 1/2 and 3/2 resonances. We also ascertained that the single beam polarization asymmetry Σ ($\mathcal{P}_{l0}^{00}$), and the double beam-target observable G ($\mathcal{P}_{lz}^{00}$) (both requiring a linearly polarized beam) are the best observables for investigating the suspected contributions of spin 5/2 resonances [11].

We also examined the strangeness photoproduction reaction, which has a rather complicated reaction mechanism [12–15]. We focused on the only available hyperon recoil polarization asymmetry P ($\mathcal{P}_{00}^{0y'}$) data [16], and showed that, if these data are confirmed by future experimental results, then s-channel spin 1/2 & 3/2 resonances are not playing a role in the reaction. This possibility would then considerably simplify the number of resonances needed in kaon photoproduction.

New physics comes in while investigating the η meson photoproduction process. Recent low-energy measurements [17,18] and the preliminary higher energy data [20] of η photoproduction lead to a very simple reaction mechanism [18,19,22]; namely, the reaction seems to be dominated by two nucleonic resonances the $S_{11}(1535)$ and $D_{13}(1520)$. This dominance suggests using η meson photoproduction to search for at least a few of the missing and/or undiscovered resonances, which have been predicted [3] to couple to the ηN rather than to the πN channels. This reaction offers a test of QCD inspired models [3,5]: namely, of predicted P_{13} and to a lesser extent D_{15} resonances with masses below, or slightly above, 2 GeV. For the P_{13} resonance(s) the recoil polarization P, which is probably rather difficult to measure, and the double polarization observable H ($\mathcal{P}_{lz}^{00}$) (which requires a polarized

target and a linearly polarized photons beam) are highly appealing. These observables offer a similar and unique selectivity among the sixteen observables; namely, their multipole polynomial expansion coefficients depend *only* on interference terms. Hence, the contributions from a sought-after P_{13} resonance is magnified by the two dominant amplitudes. Moreover, the presence of a $a_2 \neq 0$ term in the second or third order polynomials serve as an unambiguous signature for the presence of, at least, one P_{13} resonance; with two nodes expected in the case of a second order polynomial. This reasoning applies also to two other observables; namely, the single target asymmetry T and the double polarization observable F ($\mathcal{P}_{x'}^{00}$) (which involves polarized target and a circularly polarized photon beam.)

Another interesting problem in the η case concerns the role played, if any, by the Roper-resonance $P_{11}(1440)$. Our approach shows that the differential cross-section is not sensitive enough to the Roper-resonance. However, four polarization observables are very suitable for this purpose. They are, as above, the single target asymmetry T, the recoil polarization P, and the double beam-target polarization observables $H\&F$. In contrast to the P_{13} contributions leading to two nodes, the Roper-resonance will produce only one node and the deviation of that node away from 90° will give a measure of the importance of the P_{11} amplitude relative to the SD dominant resonances.

Finally, the effect of the spin 5/2 D-resonances, known or missing, show up clearly in the highest order coefficients for any of the three single polarization observables, or for any beam-target double polarization asymmetry(E, F, G, H).

In summary, some puzzles in hadron spectroscopy might be answered by studying η photoproduction. Our investigation shows that the most promising observables require asymmetry measurements with polarized beam and/or polarized target. So, final results from the recent polarized target asymmetry T measurements [24] at ELSA are awaited for. Moreover, polarized beams are becoming available at CEBAF and GRAAL and new advances in the polarized target techniques [25] are expected to render such single and even double polarization measurements feasible in the near future.

ACKNOWLEDGMENTS

We wish to thank J. Ajaka, C. Fayard, P. Girard, P. Hoffman-Rothe, and G.H. Lamot for helpful exchanges, and J.P. Didelez for his interest in this work and much encouragement. Each of us wishes to express appreciation for warm hospitality during visits to the University of Pittsburgh (B.S.) and to Saclay (F.T.).

APPENDIX A: MULTIPOLE EXPANSION FOR THE TARGET POLARIZATION

The polarized target asymmetry profile function is given here in terms of the polynomial expansion. The associated coefficients a_m are then expressed as imaginary parts of bilinear products of multipole amplitudes. This case is used to illustrate the compact notation used in Table I, wherein the general structure of spin observables for pseudoscalar meson photoproduction is displayed. The profile function $T(\theta)$ is of Legendre class $\mathcal{L}_{1b}$ and hence has the general form:

$$T(\theta) \equiv \mathcal{O}_{0y}^{00}(x) = \sin\theta \sum_{m=0}^{n} a_m x^m, \tag{A1}$$

with $x \equiv \cos(\theta)$. The polynomial expansion coefficients are expressed in terms of electric and magnetic multipole amplitudes as:

$$\begin{aligned}
a_0 &= Im[\, E_0^+[-3\,E_1^+ + 3\,M_1^+]^* - M_1^-[3\,E_2^- + 3\,M_2^- + 3\,E_2^+ - 3\,M_2^+]^* \\
&\quad + E_1^+[-6\,E_2^- - \frac{27}{2}\,E_2^+]^* + M_1^+[-6\,M_2^- + \frac{15}{2}\,E_2^+ + 6\,M_2^+]^* \,] \\
a_1 &= Im\frac{3}{2}[\, E_0^+[2\,E_2^- + 2\,M_2^- - 8\,E_2^+ + 8\,M_2^+]^* - M_1^-[-2\,E_1^+ + 2\,M_1^+]^* \\
&\quad + E_2^-[25\,E_2^+ + 2\,M_2^+]^* + M_2^-[-3\,E_2^+ + 30\,M_2^+]^* \\
&\quad + 8\,E_1^+\,M_1^{+*} + 8\,E_2^-\,M_2^{-*} - 18\,E_2^+\,M_2^{+*} \,] \\
a_2 &= Im\frac{3}{2}[\, M_1^-[10\,E_2^+ - 10\,M_2^+]^* + E_1^+[12\,E_2^- - 3\,E_2^+ + 30\,M_2^+]^* \\
&\quad + M_1^+[12\,M_2^- - 25\,E_2^+ - 2\,M_2^+]^* \,] \\
a_3 &= Im\frac{45}{2}[\, -3\,E_2^-\,E_2^{+*} + M_2^-[E_2^+ - 4\,M_2^+]^* + 6\,E_2^+\,M_2^{+*} \,]
\end{aligned} \tag{A2}$$

Expressions for all other observables are available in reference [6].

REFERENCES

* Research supported in part by the U. S. National Science Foundation.

[1] C. G. Fasano, F. Tabakin and B. Saghai, Phys. Rev. C **46**, 2430 (1992).
[2] B. Saghai and F. Tabakin, Phys. Rev. C **53**, 66 (1996).
[3] S. Capstick and W. Roberts, Phys. Rev. D **49**, 4570 (1994).
[4] S. Capstick and W. Roberts, Phys. Rev. D **47**, 1994 (1993).
[5] R. Koniuk and N. Isgur, Phys. Rev. D **21**, 1868 (1980).
[6] P. Girard, B. Saghai and F. Tabakin, Saclay Report, DAPNIA-SPhN-96-01 (1996).
[7] *See e.g., SAID database quoted in* R.A. Arndt, I.I. Strakovsky, R.L. Workman, and M.M. Pavan, Phys. Rev. C **52**, 2120 (1995).
[8] H. Dutz and the PHOENICS Collaboration, *Spin '94 Symposium*, Bloomington, 1994, Editors E.J. Stephenson and S.E. Vigdor, AIP Conference Proceedings No 339 (1995).
[9] K. Büchler *et al.*, Nucl. Phys. **A570**, 580 (1994).
[10] A.M. Sandorfi, *Spin '94 Symposium*, Bloomington, 1994, Editors E.J. Stephenson and S.E. Vigdor, AIP Conference Proceedings No 339 (1995).
[11] H. Garcilazo and E. Moya de Guerra, Nucl. Phys. **A562**, 521 (1993).
[12] R. A. Adelseck and B. Saghai, Phys. Rev. C **42**, 108 (1990).
[13] R. Williams, C. Ji, and S. Cotanch, Phys. Rev. C **46**, 1617 (1992).
[14] J.C. David, C. Fayard, G.H. Lamot, and B. Saghai, *to appear in* Phys. Rev. C.
[15] Zhenping Li, Phys. Rev. D **50**, 5639 (1994); *ibid* D **52**, 4961 (1995); Phys. Rev. C **52**, 1648 (1995).
[16] M. Bockhorst *et al.*, Z. Phys. C **63**, 37 (1994); J. Barth *et al.*, to appear in the *Proceedings of the 7th International Conference on the Structure of Baryons*, Santa Fe, 1995, editors J.B. McClelland and B.F. Gibson, World Scientific.
[17] S.A. Dytman *et al.*, Phys. Rev. C **51**, 2710 (1995); J. W. Price *et al.*, *ibid.* C **51**, R2283 (1995).
[18] B. Krusche *et al.*, Phys. Rev. Lett. **74**, 3736 (1995).
[19] M. Benmerrouche, Nimai C. Mukhopadhyay, and J.F. Zhang, Phys. Rev. D **51**, 3237 (1995).
[20] M. Rigney *et al.*, *Proceedings of the 14th International Few-Body Conference*, Williamsburg, 1994, edited by F. Gross, AIP Conference Proceedings No 334 (1995); M. Breuer, Ph.D. thesis, University of Bonn (1994); G. v. Edel, Ph.D. thesis, University of Göttingen (1995).
[21] G. Anton, J.P. Didelez, and P. Hoffmann-Rothe, *private communication* (1996).
[22] J. Ajaka, P. Hoffmann-Rothe, B. Saghai, and F. Tabakin, *in preparation.*
[23] M. Bouché-Pillon, B. Saghai, and F. Tabakin, *8th International Symposium on Polarization Phenomena in Nuclear Physics*, Bloomington, 1994, Editors E.J. Stephenson and S.E. Vigdor, AIP Conference Proceedings No 339 (1995).
[24] G. Anton and A. Bock, *private communication* (1996).
[25] J.P. Didelez, Nucl. Phys. News **4**, 10 (1994).

TABLES

TABLE I. The notation $\mathcal{P}^{meson,\ final\ baryon}_{photon,\ initial\ baryon}$ is used to indicate the initial (final) baryon $xyz(x'y'z')$ spin directions and the photon's circular(c) or linear(l) polarization.

Class	Observable	Symbol	Notation
$\mathcal{L}_0$			
	Cross-section	I	$\mathcal{P}^{00}_{00}$
	Beam-Target	E	$\mathcal{P}^{00}_{cz}$
	Beam-Recoil	$C_{z'}$	$\mathcal{P}^{0z'}_{c0}$
	Target-Recoil	$L_{z'}$	$\mathcal{P}^{0z'}_{0z}$
$\mathcal{L}_{1a}$			
	Recoil	P	$\mathcal{P}^{0y'}_{00}$
	Beam-Target	H	$\mathcal{P}^{00}_{lx}$
	Beam-Recoil	$C_{x'}$	$\mathcal{P}^{0x'}_{c0}$
	Target-Recoil	$L_{x'}$	$\mathcal{P}^{0x'}_{0z}$
$\mathcal{L}_{1b}$			
	Target	T	$\mathcal{P}^{00}_{0y}$
	Beam-Target	F	$\mathcal{P}^{00}_{cx}$
	Beam-Recoil	$O_{x'}$	$\mathcal{P}^{0x'}_{l0}$
	Target-Recoil	$T_{z'}$	$\mathcal{P}^{0z'}_{0x}$
$\mathcal{L}_2$			
	Beam	Σ	$\mathcal{P}^{00}_{l0}$
	Beam-Target	G	$\mathcal{P}^{00}_{lz}$
	Beam-Recoil	$O_{z'}$	$\mathcal{P}^{0x'}_{l0}$
	Target-Recoil	$T_{x'}$	$\mathcal{P}^{0x'}_{0x}$

TABLE II. Multipole dependence of the polynomial coefficients for all single and double polarization observables in pseudoscalar meson production. Here $i = 1$ and $i = 3$ denote the $J = 1/2$ and 3/2 P-waves ($P \equiv P_{2I_i}$ and $P' \equiv P_{2I_3}$, respectively); while $j = 3$ and $j = 5$ are the $J = 3/2$ and 5/2 D-waves ($D \equiv D_{2I_3}$ and $D' \equiv D_{2I_5}$, respectively). Single letters refer to terms of the type $|E_0^+|^2 \equiv S$; such terms are listed in the first row for each set of observables, when appropriate. In the following rows the interference terms are given in the notation $SD_{2I_j}, \cdots$. The term $P_{2I_i}D_{2I_j}$ is short for $PD \oplus PD' \oplus P'D \oplus P'D'$. The boxed letters show how the strong S-wave contributes to the a_m coefficients for each observable.

	a_0	a_1	a_2	a_3	a_4	a_5
$\mathcal{L}_0$						
$d\sigma$ & E	$\boxed{S} \oplus P_{2I_i} \oplus D_{2I_j} \oplus \boxed{SD_{2I_j}} \oplus PP' \oplus DD'$	$\boxed{SP_{2I_i}} \oplus P_{2I_i}D_{2I_j}$	$P' \oplus D_{2I_j} \oplus \boxed{SD_{2I_j}} \oplus PP' \oplus DD'$	$PD' \oplus P'D_{2I_j}$	$D' \oplus DD'$	
$C_{x'}$ & $L_{x'}$	$\boxed{SP_{2I_i}} \oplus P_{2I_i}D_{2I_j}$	$\boxed{S} \oplus P_{2I_i} \oplus D_{2I_j} \oplus \boxed{SD_{2I_j}} \oplus PP' \oplus DD'$	$\boxed{SP'} \oplus P_{2I_i}D_{2I_j}$	$P' \oplus D_{2I_j} \oplus \boxed{SD'} \oplus DD'$	$P'D'$	D'
$\mathcal{L}_{1a}$						
P & H	$\boxed{SP_{2I_i}} \oplus P_{2I_i}D_{2I_j}$	$\boxed{SD_{2I_j}} \oplus PP' \oplus DD'$	$PD' \oplus P'D_{2I_j}$	DD'		
$C_{x'}$ & $L_{x'}$	$\boxed{S} \oplus P_{2I_i} \oplus D_{2I_j} \oplus \boxed{SD_{2I_j}} \oplus PP' \oplus DD'$	$\boxed{SP'} \oplus PD_{2I_j} \oplus P'D'$	$P' \oplus D_{2I_j} \oplus \boxed{SD'} \oplus DD'$	$P'D'$	D'	
$\mathcal{L}_{1b}$						
T & F	$\boxed{SP'} \oplus P_{2I_i}D_{2I_j}$	$P' \oplus D_{2I_j} \oplus \boxed{SD_{2I_j}} \oplus PP' \oplus DD'$	$PD' \oplus P'D_{2I_j}$	$D' \oplus DD'$		
$O_{x'}$ & $T_{x'}$	$P' \ominus D_{2I_j} \ominus \boxed{SD_{2I_j}} \ominus PP' \ominus DD'$	$\boxed{SP'} \ominus P_{2I_i}D_{2I_j}$	$P' \oplus D_{2I_j} \oplus \boxed{SD'} \oplus DD'$	$P'D'$	D'	
$\mathcal{L}_2$						
Σ & G	$P' \ominus D_{2I_j} \oplus \boxed{SD_{2I_j}} \oplus PP' \ominus DD'$	$PD' \oplus P'D_{2I_j}$	$D' \ominus DD'$			
$O_{z'}$ & $T_{z'}$	$\boxed{SP'} \oplus P_{2I_i}D_{2I_j}$	$P' \ominus D_{2I_j} \ominus \boxed{SD'} \oplus DD'$	$P'D'$	D'		

TABLE III. The role of various resonance scenarios on η photoproduction. The amplitudes are assumed to be dominated by resonances. Starting from the well-known resonances $SD(S = S_{11}(1535)$ and $D_{13}(1520))$, others are added sequentially; namely, $P \equiv P_{11}(1440)$, $P' \equiv P_{13}$, $D \equiv D_{13}$, $D' \equiv D_{15}$ to generate various resonance scenarios. For each combination of resonances, and for polynomial orders of $n = 1, (a_0 + a_1 \cos\theta)$; $n = 2, (a_0 + a_1 \cos\theta + a_2 \cos^2\theta)$, etc.; the relative size of the expansion coefficients are predicted, based on Table I. A large coefficient is denoted as $a_m >>$. This information can be used to predict the effect of a given set of resonances on the angular and energy dependence of spin observables for η meson photoproduction.

Observable	$n = 1$	$n = 2$	$n = 3$	$n = 4$	$n = 5$
$\mathcal{L}_0$					
$d\sigma$ & E		SD^a	$SP'D^g$	$SPP'DD'$	
		SPD^b	$SPP'D^g$		
$C_{x'}$ & $L_{x'}$			SD^c		$SPP'DD'$
			SPD		
			$SP'D$		
			$SPP'D$		
$\mathcal{L}_{1a}$					
P & H	SD^d	$SP'D^e$	$SPP'DD'$		
	SPD^f	$SPP'D^e$			
$C_{x'}$ & $L_{x'}$		SD^a		$SPP'DD'$	
		SPD^b			
		$SP'D^b$			
		$SPP'D^b$			
$\mathcal{L}_{1b}$					
T & F	SD^d	$SP'D^e$	$SPP'DD'$		
	SPD^f	$SPP'D^e$			
$O_{x'}$ & $T_{x'}$		SD^a	$SP'D^b$	$SPP'DD'$	
		SPD^b	$SPP'D^b$		
$\mathcal{L}_2$					
Σ & G	SD^h	$SPP'DD'$			
	SPD^h				
	$SP'D^i$				
	$SPP'D^i$				
$O_{z'}$ & $T_{x'}$	SD^d		$SPP'DD'$		
	SPD^j				
	$SP'D^j$				
	$SPP'D^j$				

$^a a_0 > a_2,\ a_1 = 0$; $^b a_0 > a_2 > a_1$; $^c a_0 = a_2 = 0,\ a_1 > a_3,\ a_3$ *pure* $D-$ *wave* ; $^d a_0 = 0$; $^e a_1 >> a_0 > a_2$; $^f a_1 > a_0$; $^g a_3 \propto P'D$; $^h a_1 = 0$; $^i a_0 > a_1,\ a_1 \propto P'D$; $^j a_1 > a_0$

FIGURES

FIG. 1. Typical energy and angular dependence of a $\mathcal{L}_0$ class polarization observable asymmetry (the depicted case is for a typical double polarization observable E for kaon production). The nodal trajectory is defined as the projection of non endpoints zero values at each energy on the plane defined by the energy of the incident photon and the angle of produced meson.

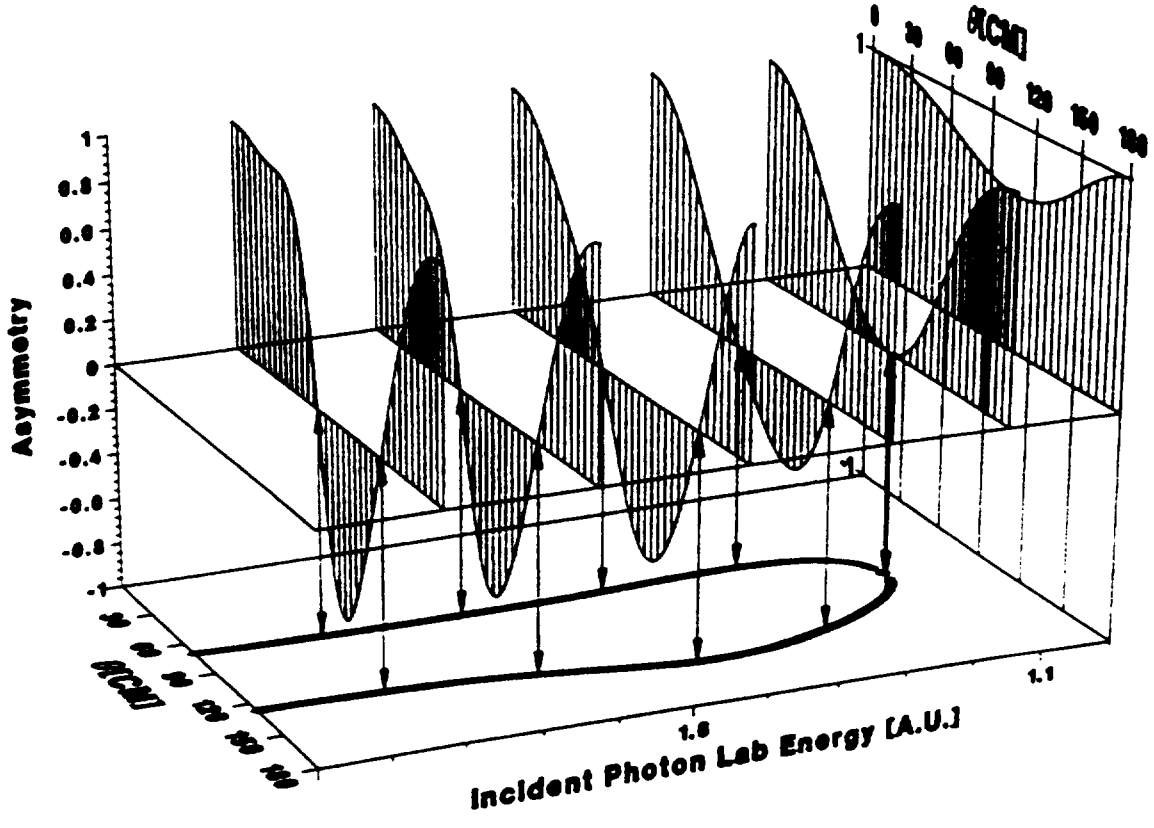

FIG. 2. Angular distribution of the polarized target asymmetry in the $\gamma\vec{p} \to \pi^+ n$ reaction at $E_\gamma^{lab} = 220$ MeV (a) and 650 MeV (b). Curves are explained in the text.

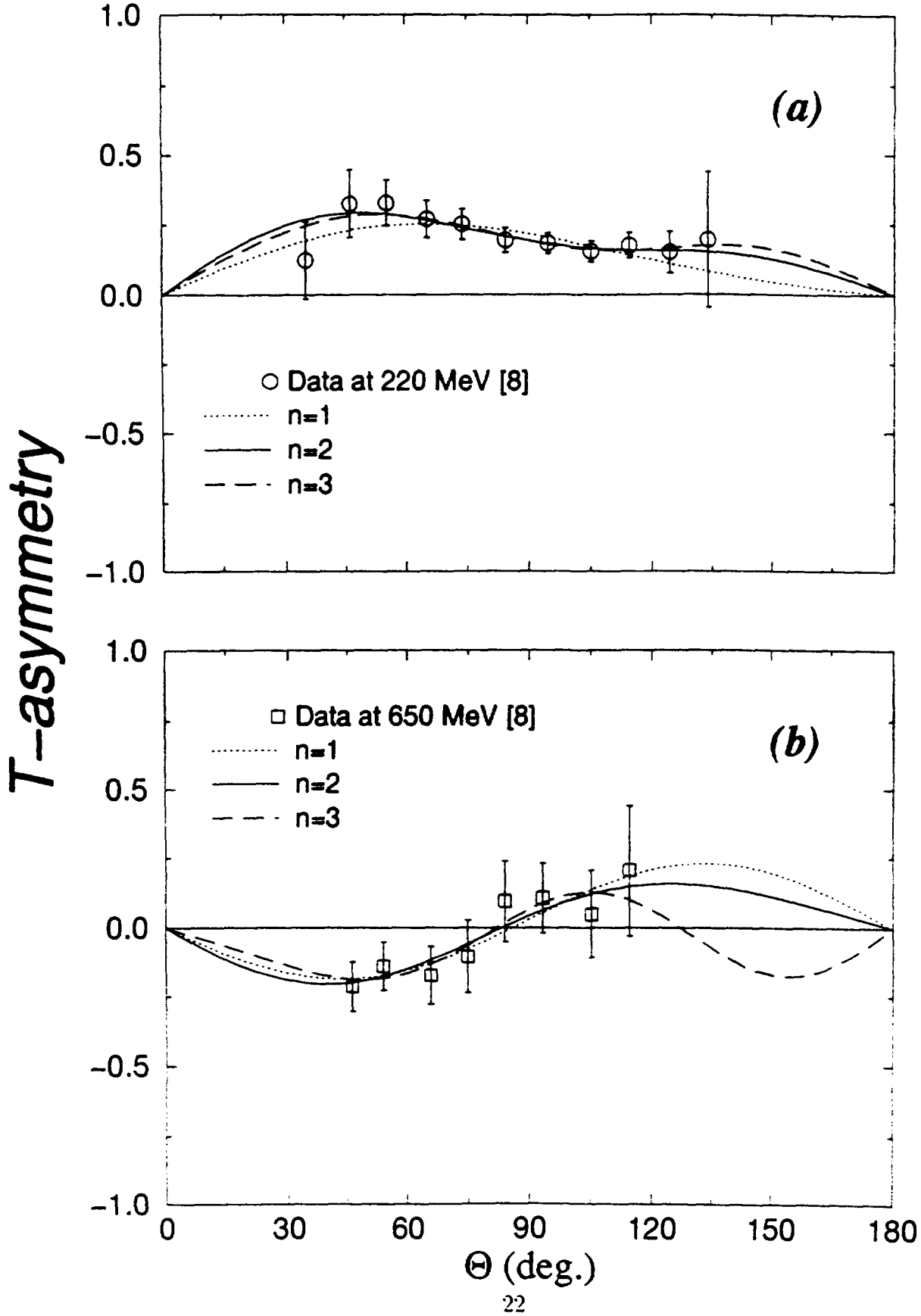

FIG. 3. Angular distribution of the recoil Λ-polarization asymmetry in the $\gamma p \to K^+\bar{\Lambda}$ channel at $E_\gamma^{lab} = 1.2$ GeV. Curves are explained in the text.